Hindawi
Advances in Materials Science and Engineering
Volume 2019, Article ID 2935942, 9 pages
https://doi.org/10.1155/2019/2935942

Research Article

Fabrication and Characteristics of Mn@ $Cu_3(BTC)_2$ for Low-Temperature Catalytic Reduction of NO_x with NH_3

Zhuo Yao,[1] **Dianli Qu**,[1] **Yuxiang Guo**,[1] **Yujing Yang**,[2] **and Hong Huang**[3]

[1]*College of Material and Metallurgy, University of Science and Technology Liaoning, Anshan, Liaoning 114001, China*
[2]*General Petrochemical Plant of Petrochina Liaohe Oilfield, Panjin, Liaoning 124022, China*
[3]*Department of Mechanical and Materials Engineering, Wright State University, Dayton, OH 45435, USA*

Correspondence should be addressed to Dianli Qu; qudianli@126.com and Hong Huang; hong.huang@wright.edu

Received 16 April 2019; Revised 14 August 2019; Accepted 16 October 2019; Published 31 October 2019

Academic Editor: Hom Kandel

Novel catalysts with high activity for the selective catalytic reduction of NO with NH_3 (NH_3-SCR) at low temperatures are highly demanded. In this study, mixed-node metal-organic frameworks (MOFs), e.g. Mn@CuBTC with controlled Mn composition in $Cu_3(BTC)_2$, were fabricated using postsynthetic exchange method and their structural characteristics and catalytic performances for NH_3-SCR reaction were assessed. A series of analyses in terms of structure, surface morphology, texture, and chemical state determined that Mn ions were successfully incorporated into the $Cu_3(BTC)_2$ crystal lattice as well as adsorbed on the walls of nanopores in the framework. The pore sizes can be finely tuned in the presence of Mn ions in the cages, which significantly suppressed water adsorption. The NH_3-SCR activity of Mn@CuBTC exhibited nearly 100% NO_x conversion rate in the temperature range (230–260°C). The superior NH_3-SCR performance is attributed to the proper pore sizes, reduced water content, and the synergistic effect between manganese and copper ions in the MOF structure, which enhanced NH_3 bound to the active Lewis sites.

1. Introduction

In the efforts of removing air-polluting nitric oxide (NO_x) gases, selective catalytic reduction (SCR) with NH_3 is a cost-effective and efficient approach. At present, most industries rely on catalysts such as V_2O_5-WO_3/TiO_2 operable in a narrow temperature window of 300–400°C, which results in inevitable technical challenges and low N_2 selectivity [1–4]. Novel catalysts with high SCR activity at temperatures lower than 300°C are highly demanded. Transition metal oxide-based catalysts present enormous potentials and their low-temperature NH_3-SCR activities are exhibited in the following order Mn > Cu > Cr >> Co > Fe >> V >> Ni [5–13]. Manganese-based catalysts are superior, which can be attributed to the versatile valence states and excellent redox ability. Multiple catalytic oxides supported on stable high-surface materials can further enhance the low-temperature performances via modified active sites, synergistic effects between the two metal ions, and metal-support interaction [14, 15]. For instance, MnO_x—CeO_x hybrid nanocatalysts supported on graphene aerogel exhibited 80% NO conversion at 150°C and 98% at 250°C [15]. Recently, Boningari et al. reported metal oxide confined in titania nanotube (M/TNT) system and noticed that the surface texture and tubular morphology greatly promote the NO_x conversion in the temperature regime of 100–300°C [16].

The emerging metal-organic frameworks (MOFs) have attracted much attention in gas separation, absorption, sensing, and catalytic reaction [17–19]. MOFs are compounds made up of metal ions coordinated with organic ligands into clusters arranged in a periodic pattern, resulting in a crystalline structure with well-defined cavities. MOFs are advantageous in terms of stable framework integrity, large nanopore volume, highly dispersed active sites, and tunable chemical structure, rendering its great candidacy as either an active catalyst or catalyst supporter. Copper benzene—1, 3, 5—tricarboxylate, i.e. $Cu_3(BTC)_2$ (abbreviated as CuBTC in this paper), has a three-dimensional

channel structure connecting a system of cages in the size of 0.3–1.2 nm with high specific surface area (up to 1400 m^2/g) and open metal active sites. According to Sun et al. [20], CuBTC performed best in adsorption of NO_x from a mixing hazardous gas. CuBTC modulated with acetic acid resulted in 95.5% NO conversion in NH_3-SCR reaction at 280°C, which is better than untreated CuBTC (60% conversion) and derived copper oxide (83.9% conversion) [21]. CuBTC activated in vacuum [22] demonstrated nearly 100% conversion of NO at temperatures from 220°C to 280°C. Qin investigated performances of the mixed-node MOFs, e.g., A-Cu-BTC series (A = Fe, Ni, Co, Mn, Sr, La, Ce, Al) and their derived oxides in the SCR of NO with CO [23]. Although the A-Cu-BTC did not perform better than Cu-BTC, the doping elements present in the CuO_x/C enhanced reactive activity and reduced the operating temperature.

This research is directed to fabricate Mn@CuBTC with controlled Mn composition in CuBTC and to assess the impacts of addition of Mn on the SCR of NO with NH_3, which has not been reported in public reports. In oxide-based catalysts, the synergistic effect between Mn and Cu ions effectively enhanced NO conversion at low temperatures [24–26]. In this study, the Mn@CuBTC series were fabricated *via* a postsynthetic exchange (PSE) method. Their structural, morphological, and compositional properties were systematically analyzed. The deNO_x capability and thermal stability of the novel catalysts Mn@CuBTC were assessed. The states of NH_3 adsorbed on the catalyst as exposed or in the presence of NO were discussed.

2. Experimental Aspects

2.1. Catalyst Synthesis. Copper nitrate trihydrate ($Cu(NO_3)_2{\cdot}3H_2O$) and manganese chloride tetrahydrate ($MnCl_2{\cdot}4H_2O$) were purchased from Sinopharm Chemical Reagent Co., Ltd (Shanghai, China). 1, 3, 5—benzene tricarboxylic acid (H_3BTC) and *N*, *N*-dimethyl formamide (DMF 99%) were purchased from Aladdin Bio-Chem Technology Co., Ltd (Shanghai, China). All chemicals were used without further purification.

CuBTC was synthesized using the hydrothermal method. Typically, $Cu(NO_3)_2{\cdot}3H_2O$ (4.5 mmol) and H_3BTC (4.5 mmol) were dissolved in a mixed solution of deionized (DI) water (15 ml), absolute ethyl alcohol (15 ml), and DMF (15 ml). The solution was placed in a 100 ml Teflon-lined autoclave and held at 120°C for 24 h. Afterwards, the obtained blue crystals were collected with the help of centrifugation and washed using DI water repeatedly to remove the unreacted chemicals. Finally, the CuBTC powders were dried at 100°C under vacuum overnight.

The as-synthesized CuBTC (0.5 g) was dispersed in 20 ml ethanol under ultrasonication for 20 min. Meanwhile, $MnCl_2{\cdot}4H_2O$ was dissolved in 50 ml ethanol to obtain solutions with different Mn^{2+} concentrations (0.01 mol/L, 0.02 mol/L, 0.05 mol/L, 0.08 mol/L, and 0.1 mol/L). Each Mn^{2+} solution was then added dropwise into one CuBTC suspension solution under vigorous stirring at room temperature for 2 h. The sample was kept in a stainless steel autoclave with a polytetrafluoroethylene liner at 90°C for 24 h. After cooling down to room temperature, the sample was filtered and washed with ethanol and DI water. Same as CuBTC, the series Mn-doped products were dried in a vacuum oven at 100°C overnight. The resulting catalysts are denoted as Mn@CuBTC-X (*X* is the nominal concentration of Mn^{2+} solution).

2.2. Catalyst Characterizations. The crystal structures, morphologies, composition, and bonding state and valency of the elements in the catalysts were analyzed by using X-ray diffraction (XRD, PANalytical X'pert with Cu Kα $\lambda = 0.154178$ nm), field emission scanning electron microscopy (FESEM, ZEISS-ΣIGMA HD), and X-ray photoelectron spectroscopic (XPS, Thermo-Fischer ESCALAB250Xi, Thermo-Fischer, U.S), respectively. For better SEM images, a few nanometer-thick gold was coated on the powder samples to reduce the charging effect.

The textural properties of the catalysts were determined using N_2 adsorption at −196°C with JW-BK 112 physisorption apparatus (JWGB Sci & Tech, China). Brunauer–Emmett–Teller (BET) and Barrett–Joyner–Halenda (BJH) methods were applied to calculate the specific surface area and pores size distribution, respectively.

Table 1 lists the texture properties and atomic percentage of each element (based on XPS analysis) in the CuBTC and Mn@CuBTC-X catalysts.

2.3. Catalyst Thermal Stability, SCR Activity, and In Situ Reaction Analyses. The thermal stability of the catalysts was determined by thermogravimetry (TG, Netzsch STA449F3) in the temperature range of 30°C to 550°C at a rate of 10°C/min under nitrogen atmosphere.

Prior to the SCR activity test, CuBTC and Mn@CuBTC-X samples were all heated at 230°C for 60 min in a flow of He to remove moisture and to activate the catalyst. The SCR activities were assessed by placing 2 mL of the activated catalyst on a fixed-bed reactor. Tests were performed in the temperature range of 150°C to 300°C using a simulating gas consisting of 500 ppm NO, 500 ppm NH_3, 5 vol.% O_2, and balanced with nitrogen at a gas space velocity of 30,000 h^{-1}. The concentration of NO_2 and N_2O in the effluent gas was determined by a Nicolet iS50 FT-IR spectrometer. Details have been described elsewhere [15]. The NO conversion and N_2 selectivity were calculated as follows:

$$\text{NO conversion (\%)} = \frac{[\text{NO}]_{\text{in}} - [\text{NO}]_{\text{out}}}{[\text{NO}]_{\text{in}}} \times 100,$$

$$\text{N}_2\text{ selectivity (\%)} = \left(\frac{[\text{NO}]_{\text{in}} + [\text{NH}_3]_{\text{in}} - [\text{NO}_2]_{\text{out}} - 2[\text{N}_2\text{O}]_{\text{out}}}{[\text{NO}]_{\text{in}} + [\text{NH}_3]_{\text{in}}}\right) \times 100. \quad (1)$$

In situ diffuse reflectance infrared Fourier transform spectroscopy (DRIFTS) was performed on Nicolet Nexus spectrometer equipped with a MCT detector. Prior to the experiment, the Mn@CuBTC-0.05 sample was heated at 230°C for 60 min in a flow of He to remove moisture and to

Table 1: Texture properties and relative elemental composition of CuBTC and Mn@CuBTC-X.

Samples	Atomic ratio	Texture properties			Atomic concentration (%)			
	Mn/Cu	Surface area (m^2/g)	Average pore size (nm)	Pore volume (cm^3/g)	C	O	Cu	Mn
CuBTC	0	1440	0.57	2.41	58.9	33.9	7.3	—
Mn@CuBTC-0.01	0.39	993	0.50	2.38	56.7	33.6	7.1	2.8
Mn@CuBTC-0.02	0.39	876	0.51	2.39	55.8	34.3	7.2	2.8
Mn@CuBTC-0.05	0.43	767	0.48	2.42	56.4	33.9	6.8	2.9
Mn@CuBTC-0.08	0.43	661	0.42	2.18	55.8	34.1	7.1	3.0
Mn@CuBTC-0.1	0.51	434	0.35	2.26	55.8	33.6	7.2	3.4

activate the catalyst. The sample was then exposed to 500 ppm NH_3/N_2 at 230°C for 30 min followed by N_2 purging for 30 min. Afterwards, 500 ppm NO^+ 5% O_2/N_2 was introduced to the NH_3-adsobred catalyst. The spectra were collected prior to any exposure, exposed to NH_3 after 10 min and 30 min, and exposed to NO at 2 min, 10 min, 30 min, and 60 min.

3. Results and Discussion

Figures 1(a) and 1(b) show the typical SEM images of the as-synthesized CuBTC and Mn@CuBTC-0.05. Most particulates exhibit well-defined octahedral crystallite with edge length in the range of 2–12 microns. Thermal activation at 230°C generates more rough and porous surface on each crystal plane (see Figures 1(c) and 1(d)). Both the bulk and surface of Mn@CuBTC-0.05 sample were further examined with the help of EDX and XPS, and both confirmed the existence of manganese in the octahedral crystal, as seen in Figures 1(e) and 1(f).

Figure 2(a) presents the experimental XRD results of Mn@CuBTC-X and CuBTC and compared the simulated CuBTC XRD profiles (Figure 2(b)). The sharp and strong diffraction peaks indicate good crystallization of the products. The peaks positioned at 6.7°, 9.5°, 11.6°, 13.4°, 19.1°, and 26.0° are in good agreement with the simulated and other published results [27], which are diffracted from planes (2 2 0), (2 2 2), (4 0 0), (4 4 0), and (0 4 0), respectively. The patterns of Mn@CuBTC-X samples exhibit similar features to CuBTC, confirming the fact that the CuBTC framework was not altered with the manganese ion exchange/addition. No reflection peaks from manganese oxides were detected in the XRD profiles. It is noteworthy that one small peak at 5.9° shows up in the Mn@CuBTC-X XRD spectra and becomes more significant at higher Mn content. This peak is known to be related with the degree of hydration. When more water presented in the CuBTC framework, the intensity of the peak reduced significantly, which can be invisible. Figure 2(b) plots the simulated XRD based on the dehydrated and hydrated CuBTC structures proposed by Wong-Ng et al. [27]. The present results suggest that Mn addition will reduce the water absorption/retaining in the MOF framework.

Figure 3(a) shows the NO conversion efficiency obtained at different temperatures in the presence of CuBTC or Mn@CuBTC catalysts. All the catalysts exhibit similar trend as a function of temperature. The NO conversion efficiency is low at 150°C and increases exponentially upon increasing the temperature from 150°C to 220°C. The NO conversion efficiency reaches maximum within the temperature window between 230°C and 260°C. When the temperature is further increased, the NO conversion efficiency starts to decrease sharply due to the decomposition of the frameworks. As seen in Figure 3(a), adding manganese in the CuBTC framework significantly increased the SCR performance. Below 200°C, the conversion efficiency using Mn@CuBTC is over 35% higher than using CuBTC manifesting the benefits of the presence of manganese. In the optimal temperature window of 230°C–260°C, the Mn@CuBTC catalysts result NO conversion over 90% with Mn@CuBTC-0.05 and Mn@CuBTC-0.08 and having the highest conversion efficiency close to 100%. Furthermore, as seen in Figure 3(b), the high N_2 selectivity (nearly 100%) over all the prepared catalyst samples can be obtained in the whole temperature range. The CuBTC and Mn@CuBTC-0.1 displayed relative lower N_2 selectivity, which proceeds to decline at about 260°C.

To gain insight of the significant performance improvement in the presence of Mn in the MOF catalysts, Mn@CuBTC-0.05 catalyst is subjected to further analysis in chemical states of Cu and Mn, phase transition upon increasing temperature, as well as the gas-absorption states on the catalysts upon exposure at the operating temperature.

Figure 4(a) shows the XPS spectrum in the Cu 2p region. The two main peaks located at 933.4 eV and 953.5 eV are characteristic of Cu $2p_{3/2}$ and Cu $2p_{1/2}$ of Cu^{2+}, respectively. The satellite peaks in the vicinity, located at 939 eV, 943 eV, and 961.6 eV, are attributed to shake up satellite peaks of Cu^{2+}. According to Yong et al., the strong copper shake up satellite peaks contributes greatly to the NH_3-SCR reaction [28]. As seen in Figure 4(b), Mn 2p spectrum exhibits two peaks ascribed to Mn $2p_{3/2}$ and Mn $2p_{1/2}$, respectively. The Mn $2p_{3/2}$ peak can be deconvoluted into two peaks centered at 641.0 eV and 644.2 eV, which indicate the presence of Mn^{3+} and Mn^{4+} ions [29–31]. Xin et al [32] has suggested that Mn^{3+} could activate NH_3 into NH_2 intermediate that will readily react with NO to produce N_2. Previous studies also confirmed that ample amount of Mn^{4+} ions is one of the key factors enhancing NH_3 oxidation in the NH_3-SCR process due to the strong oxidizing state of Mn (IV) [15, 16].

Figure 5 presents the mass change of Mn@CuBTC-0.05, compared with CuBTC, upon increasing temperature. In general, two characteristic stages transitioned around 300°C are observed in both samples. At low-temperature region (below 270°C), the weight loss is due to the volatilization of adsorbed water in the framework cages. For Mn@CuBTC-0.05, the weight loss is 7.3% at 150°C, which is equivalent to $x = 2.64$ of hydrated water. In contrast, the weight loss is 12%

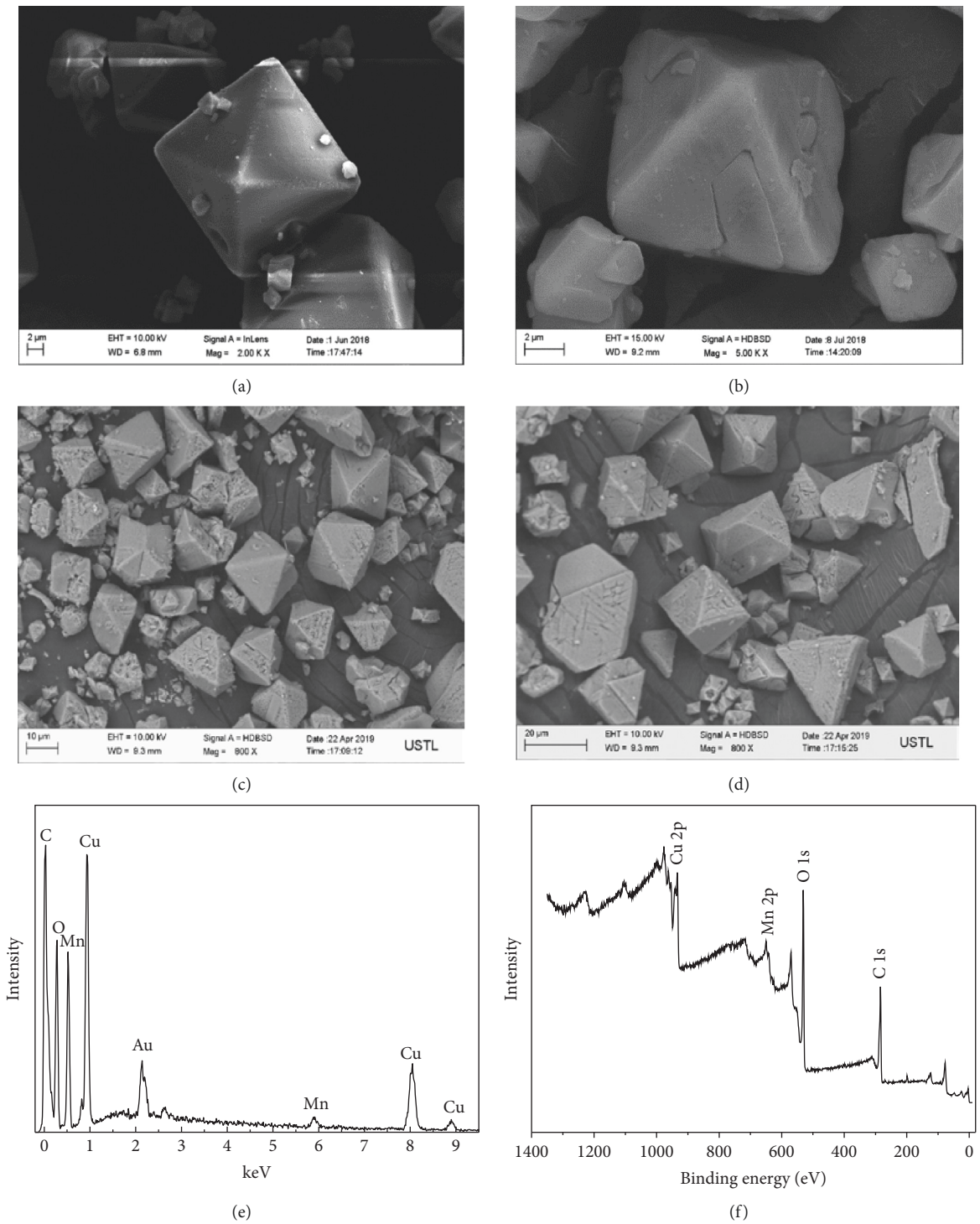

Figure 1: Representative SEM images of (a) as-prepared CuBTC, (b) as-prepared Mn@CuBTC-0.05, (c) activated CuBTC, and (d) activated Mn@CuBTC-0.05; representative survey of (e) EDS spectrum and (f) XPS spectrum obtained from as-prepared Mn@CuBTC-0.05.

equivalent to $x = 4.58$ hydrated water. This observation indicates that the as-prepared Mn@BTC has much less water content in the framework, consisting XRD results discussed in the previous session.

In the temperature range of 200°C to 270°C, the mass remains approximately unchanged, suggesting that all the hydrated water molecules are removed from the crystal while the framework is still stable. This temperature region corroborates well with the high NO conversion observed in Figure 3. In the CuBTC framework, the binuclear Cu_2-clusters are coordinated with four carboxylate groups per copper to form a paddle-wheel unit. The Cu^{2+} ions are connected through a weak bond and the residual axial coordination site can readily attract water molecule [33, 34].

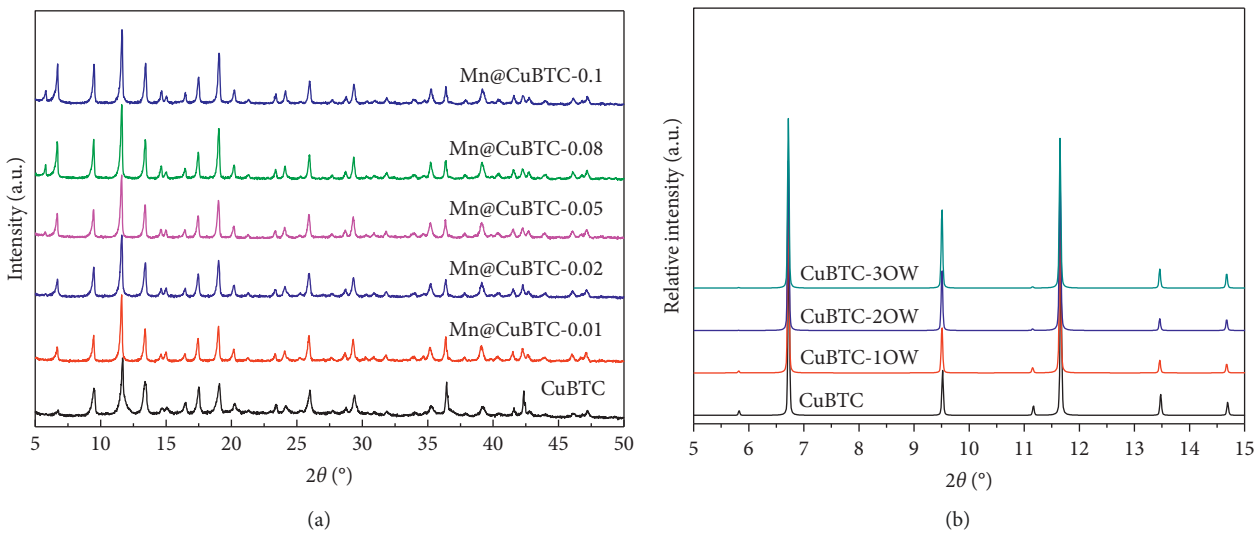

Figure 2: XRD profiles of (a) experimental results obtained from CuBTC and Mn@CuBTC-X in this study; (b) simulated CuBTC with different amount of water presented in three sites in the framework (based on the structural parameters reported in [27]).

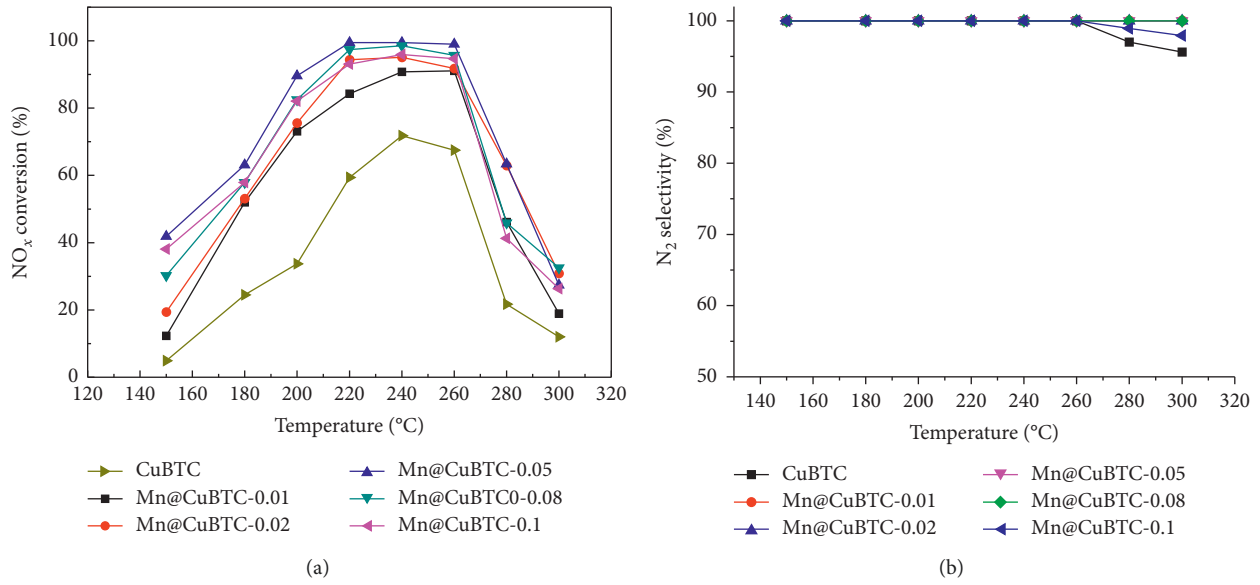

Figure 3: NO conversion efficiency (a) and N_2 selectivity (b) of CuBTC and Mn@CuBTC-X catalysts as a function of temperatures. Reaction conditions: 500 ppm NO, 500 ppm NH_3, 5 vol.% O_2, and N_2 balance, GHSV = 30,000 h^{-1}.

Wong-Ng et al. [27] proposed three different sites for water molecule occupancy (see Figure 6). In addition to weakly bounded to the coordination sites, extra water can be adsorbed on the main cage wall as well as the center of the main cage. Since both copper active site and nanopores are filled with water, the hydrated CuBTC has poor catalytic activity. From the TG results, it is seen that the water molecules in the pore center and wall can readily desorb around 100°C in CuBTC. In Mn@CuBTC-0.05, Mn addition significantly suppressed the water adsorption in the framework, which may to be attributed to a portion of Mn ions occupying water adsorption/coordination sites in addition to substitution of the copper. Water molecules occupying the coordination sites will require more energy to remove up to 200°C. Upon complete removal of water molecules from the framework while the MOF framework remains integrity, a large number of Lewis acid coordination sites on the catalytic ions are exposed when the catalytic activity becomes maximum as observed in CuBTC and Mn@CuBTC in the temperature window of 230–260°C. It is submitted that the suppression of water adsorption as well as the presence of Mn in both the active and surface sites may synergistically improve the catalytic activity at low temperatures.

The dramatic weight loss at 270°C and 330°C corresponds to the decomposition of the BTC organic linkers. In the same temperature range, the catalytic activity also rapidly decreased, which can be ascribed to the collapse and

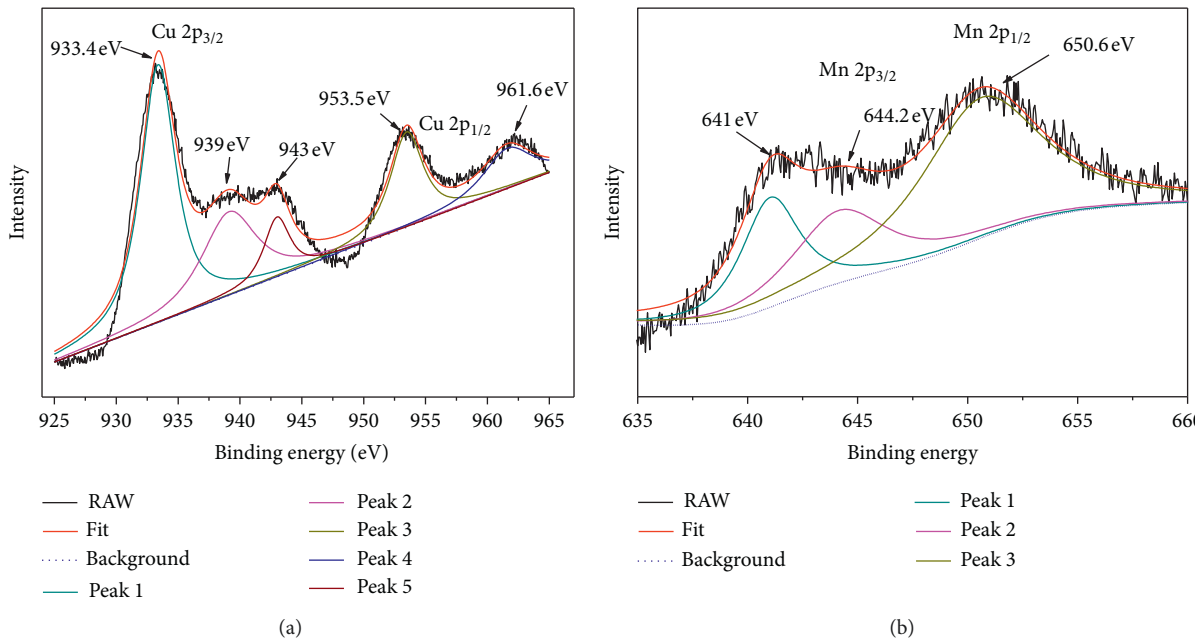

Figure 4: Representative XPS spectra with deconvoluted and fitting results. (a) Cu 2p region and (b) Mn 2p for Mn@CuBTC-0.05.

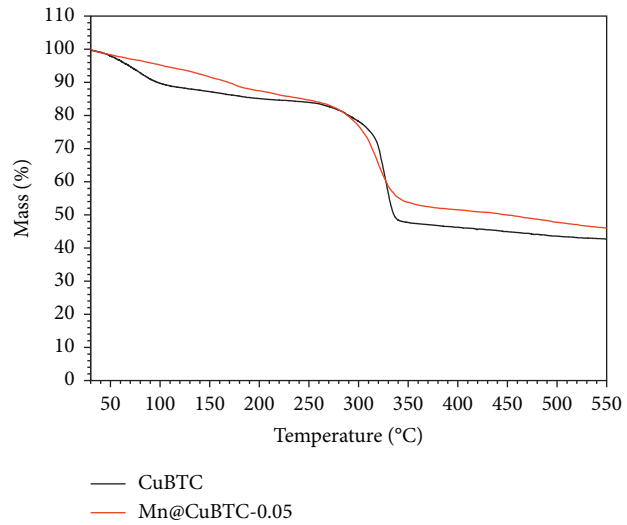

Figure 5: TG curves showing the mass loss as a function of temperature in the range of 30°C to 550°C, obtained from as-prepared CuBTC and Mn@CuBTC-0.05 samples.

decomposition of framework in CuBTC as well as in Mn@CuBTC. As the temperature increased to 350°C, only 47.7% of the mass remains in CuBTC. The weight loss value suggests that the decomposition product at this stage is the copper carbonates. The carbonates will gradually decompose into CuO, manifesting with the gradual weight loss between 370°C and 550°C. The slightly higher mass in the decomposed products in Mn@CuBTC is due to the extra amount of manganese. It is reported that CuBTC has completely decomposed into CuO_x, which showed good SCR catalytic activities [23]. The catalytic activities of the calcined BTC compounds are beyond the scope of this research.

Furthermore, appropriate pore size may be another key factor facilitating the adsorption of NO and accelerating the reaction rate. As seen in Table 1, with the continuously increase of Mn dopant amount, the pore size gradually reduced from 0.57 nm to 0.35 nm. It needs to be noted that both the specific surface area the samples gradually decreased with the increasing Mn ions concentration. However, the catalytic activity of Mn@CuBTC-X is highest when $X = 0.05$–0.08. These results suggested that the cage pore size, compared with the BET specific surface area, is a more crucial factor affecting the NH_3-SCR catalytic activity. It is interesting to see from this study that cage pore size can be finely tuned via Mn doping.

In situ DRIFTS experiments were used to detect the species absorbed on the surface of catalysts and to gain insight of the SCR reaction mechanism. Figures 7(a) and 7(b) show the DRIFT spectra of Mn@CuBTC-0.05 at different situations. Prior to any gas exposure, the majority of vibrational bands (see Figure 7(a)) are concentrated in the range of 1300–1700 cm^{-1} from symmetric and asymmetric stretching modes in the carboxylate groups. The peak in the vicinity of 1650 cm^{-1} reflects the carboxylate linking with metal ions in the form of chelation or bidentate ligand. A few peaks in 700–800 cm^{-1} reflect C-H stretching modes. The series peaks in the fingerprint area are the benzene ring characteristics [35]. The duplet peaks may reflect the coexistence of Mn and Cu in the framework causing different extent shift of the peaks. No water-related peaks are observed, which confirmed the complete dehydration of Mn@CuBTC-0.05 after activation treatment at 230°C.

Upon exposure to NH_3, as seen in Figure 7(a), several peaks emerge at 1101 cm^{-1}, 1252 cm^{-1}, 1385 cm^{-1}, 1670 cm^{-1}, 2930 cm^{-1}, and 3500 cm^{-1}. These peaks reflect a series of vibrational modes of different states of NH_3 [36–38]. For

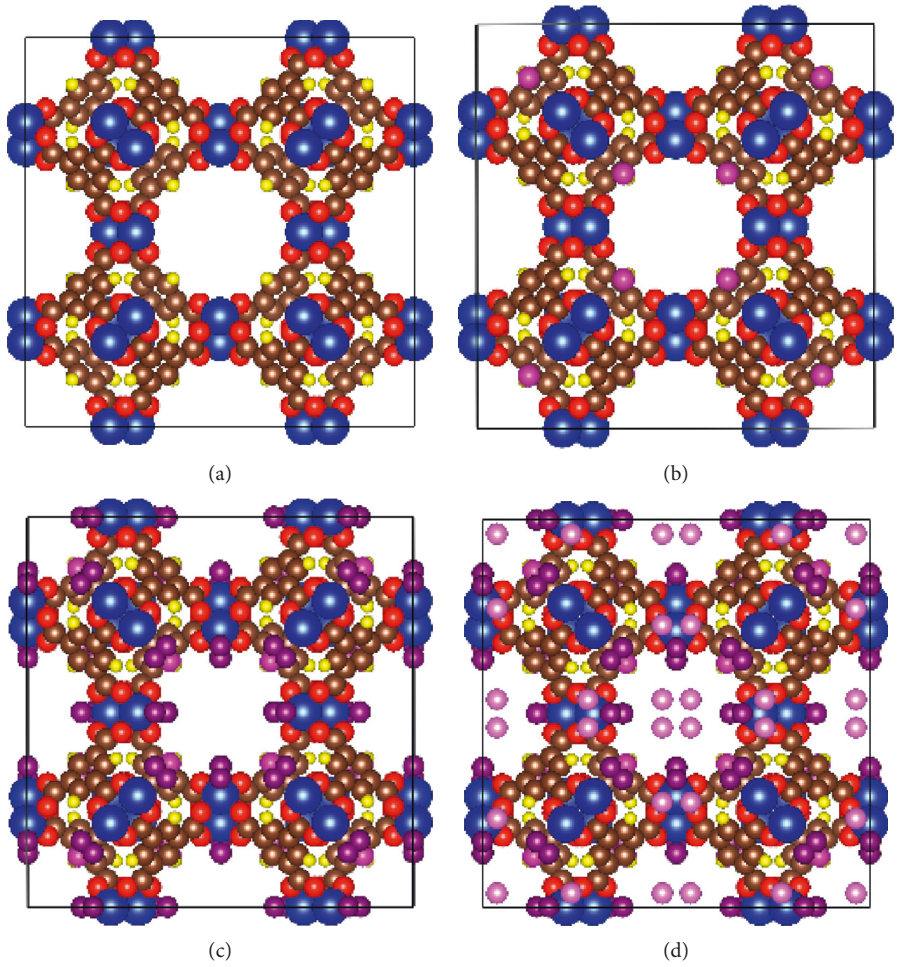

Figure 6: Schematics of the structure of (a) dehydrated CuBTC; (b) hydrated CuBTC with OW1; (c) hydrated CuBTC with OW1 and OW2; (c) hydrated CuBTC with OW1, OW2, and OW3. Symbols: Cu (blue), O (red), C (brown), H (yellow), OW1 (pink), OW2 (purple), and OW3 (light pink).

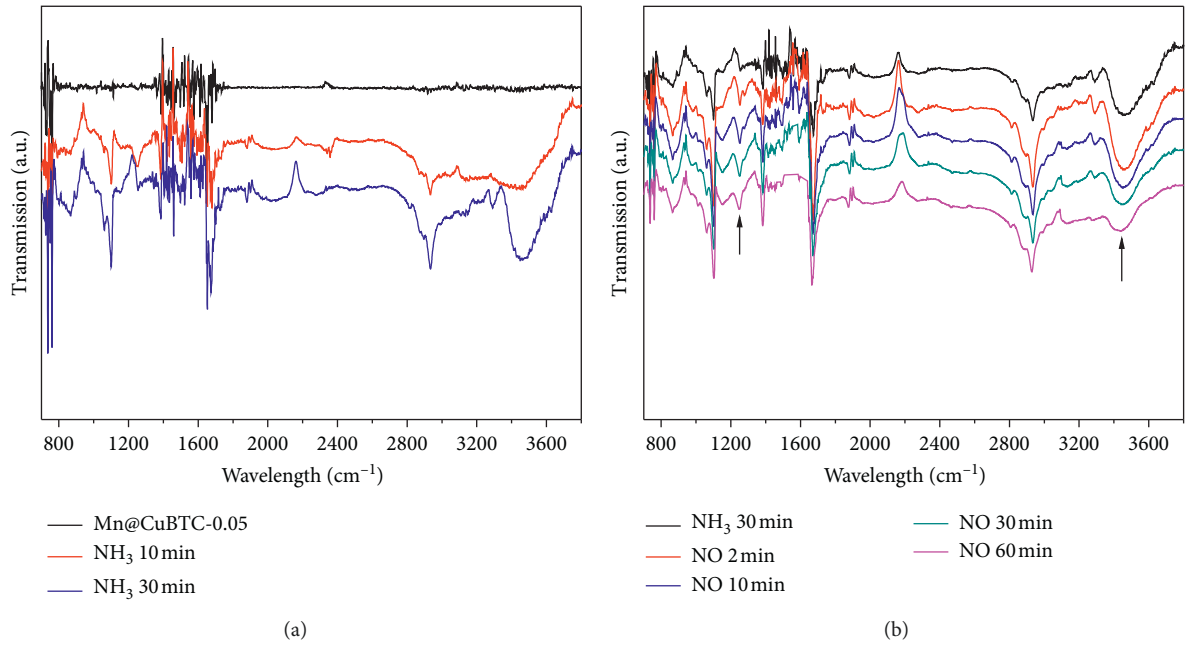

Figure 7: In situ DRIFT spectra of activated Mn@CuBTC-0.05 (a) exposed to NH_3 at 230°C for 10 min and 30 min in comparison with no exposure. Reaction condition: $[NH_3] = 500$ ppm, and N_2 balance; (b) exposed to $NO + O_2$ at 230°C for various times after NH_3 adsorption and purged with N_2. Reaction condition: $[NO] = 500$ ppm, $[O_2] = 5\%$ and N_2 balance.

instance, the broad bands centered at 3500 cm^{-1} and the small peak at 1252 cm^{-1} can be attributed to the stretching vibrations of NH_3 adsorbed on the Lewis acid sites in the catalysts. The broad peak centered at 2930 cm^{-1} may be related to vibration of second layer NH_3 atop of NH_3 strongly bound to the catalyst. No peaks at 1610 cm^{-1} and 1450 cm^{-1} were observed, indicating the significant difference between Mn@CuBTC from MnO_x-based catalysts. By contrast, the strong peaks that appear at 1670 cm^{-1} and 1385 cm^{-1} related to the stretching and bending of NH_3 bound to the carboxylate ligand, i.e. the Bronsted acid sites. The 1101 cm^{-1} peak corresponds to the N-H wagging on the catalysts. In brief, it can be submitted that the NH_3 species absorbed on the surface of catalysts exists in versatile forms. As the NH_3 exposure time increased from 10 to 30 minutes, the intensity of all these peaks increased, indicating that more NH_3 species were adsorbed on the catalyst.

When $NO + O_2$ gases are supplied to the Mn@CuBTC-0.05 preadsorbed with NH_3, it is interesting to note that all the above peaks remained (see Figure 7(b)). However, the relative intensity is different. Normalized to the strongest peak at 1670 cm^{-1}, the intensities of the 3500 cm^{-1} and 1252 cm^{-1} peaks reduced gradually while the catalytic reactions proceed. This result suggests that N-H groups bound to the Lewis sites in the catalyst, instead of NH_3 bound to Bronsted sites and weakly adsorbed on the catalyst surface, play the dominant role in the SCR reaction. No peaks corresponding to NO were observed in the DRIFT spectra. This phenomenon may suggest that either the NO species that participate in the reaction in the gaseous phase or the peaks of the intermediate phases overlap with the main NH_3 peaks, which is indistinguishable [37, 38]. Furthermore, there are no characteristic peaks of N_2O observed, suggesting a relatively high N_2 selectivity at the operating temperatures.

4. Conclusion

A series of novel catalysts Mn@CuBTC are successfully synthesized via postsynthetic exchange approach. Mn ions were homogeneously incorporated in CuBTC crystals and adsorbed on the surface of the walls of nanopores. The average pore size can be finely tuned by controlling the Mn composition. The presence of Mn ions reduces the water occupancy in the MOF nanopores. Compared with CuBTC, the SCR performance of Mn@CuBTC significantly increased, e.g., about 40% at 180°C. In the optimal temperature window of 230°C–260°C, the novel Mn@CuBTC catalyst has a highest conversion rate close to 100%. The superior NH_3-SCR performance is attributed to the proper pore sizes, enhancement of redox activity from strong oxidizing Mn^{4+} ions, as well as a synergistic effect between Mn and Cu ions in the MOF structure. In the process of NH_3-SCR reaction, ammonia reduces NO via absorbing on the Lewis sites on surface of Mn@CuBTC catalysts.

Data Availability

Raw data were generated at corresponding facilities described in the paper. Derived data supporting the findings of this study are available from Zhuo Yao on request via email (yaozhuo1986@163.com).

Conflicts of Interest

The authors declare that there are no conflicts of interest regarding the publication of this paper.

Acknowledgments

The financial support of National Science-Technology Support Plan Projects of China (no. 2014BAB02B03) and Liaoning Magnesium Industry Collaborative Innovation Center of University of Science and Technology Liaoning (no. USTLX201801) is gratefully acknowledged.

References

[1] I. Nova, L. Lietti, E. Tronconi, and P. Forzatti, "Dynamics of SCR reaction over a TiO_2-supported vanadia-tungsta commercial catalyst," *Catalysis Today*, vol. 60, no. 1-2, pp. 73–82, 2000.

[2] M. Casanova, E. Rocchini, A. Trovarelli, K. Schermanz, and I. Begsteiger, "High-temperature stability of V_2O_5/TiO_2-WO_3-SiO_2 SCR catalysts modified with rare-earths," *Journal of Alloys and Compounds*, vol. 408–412, pp. 1108–1112, 2006.

[3] X. Shang, G. Hu, C. He et al., "Regeneration of full-scale commercial honeycomb monolith catalyst (V_2O_5–WO_3/TiO_2) used in coal-fired power plant," *Journal of Industrial and Engineering Chemistry*, vol. 18, no. 1, pp. 513–519, 2012.

[4] C. Qi, W. Bao, L. Wang, and H. Li, W. Wu, Study of the V_2O_5-WO_3/TiO_2 catalyst synthesized from waste catalyst on selective catalytic reduction of NO_x by NH_3," *Catalysis*, vol. 7, no. 4, p. 110, 2017.

[5] T. Boningari and P. G. Smirniotis, "Impact of nitrogen oxides on the environment and human health: Mn-based materials for the NO_x abatement," *Current Opinion in Chemical Engineering*, vol. 13, pp. 133–141, 2016.

[6] M. Fu, C. Li, P. Lu et al., "A review on selective catalytic reduction of NO_x by supported catalysts at 100–300°C—catalysts, mechanism, kinetics," *Catalysis Science & Technology*, vol. 4, no. 1, pp. 14–25, 2014.

[7] G. Qi, R. T. Yang, and R. Chang, "MnO_x-CeO_2 mixed oxides prepared by co-precipitation for selective catalytic reduction of NO with NH_3 at low temperatures," *Applied Catalysis B: Environmental*, vol. 51, no. 2, pp. 93–106, 2004.

[8] F. Cao, J. Xiang, S. Su, P. Wang, S. Hu, and L. Sun, "Ag modified Mn–Ce/γ-Al_2O_3 catalyst for selective catalytic reduction of NO with NH_3 at low-temperature," *Fuel Processing Technology*, vol. 135, pp. 66–72, 2015.

[9] S. M. Lee, K. H. Park, and S. C. Hong, "MnO_x/CeO_2–TiO_2 mixed oxide catalysts for the selective catalytic reduction of NO with NH_3 at low temperature," *Chemical Engineering Journal*, vol. 195-196, pp. 323–331, 2012.

[10] J. Li, J. Chen, R. Ke, C. Luo, and J. Hao, "Effects of precursors on the surface Mn species and the activities for NO reduction over MnO_x/TiO_2 catalysts," *Catalysis Communications*, vol. 8, no. 12, pp. 1896–1900, 2007.

[11] Z. Tong, X. Lu, and C. Song, "The CeO_x and MnO_x nanocrystals supported on TiO_2–graphene oxide catalysts and their selective catalytic reduction properties at low temperature," *Crystals*, vol. 7, no. 6, p. 159, 2017.

[12] D. Damma, P. R. Ettireddy, B. M. Reddy, and P. G. Smirniotis, "A review of low temperature NH_3-SCR for removal of NO_x," *Catalysts*, vol. 9, no. 4, p. 349, 2019.

[13] D. Damma, T. Boningari, P. R. Ettireddy, B. M. Reddy, and P. G. Smirniotis, "Direct decomposition of NO_x over TiO_2 supported transition metal oxides at low temperatures," *Industrial & Engineering Chemistry Research*, vol. 57, no. 49, pp. 16615–16621, 2018.

[14] T. Boningari, P. R. Ettireddy, A. Somogyvari et al., "Influence of elevated surface texture hydrated titania on Ce-doped Mn/TiO_2 catalyst for the low temperature SCR of NO_x under oxygen-rich conditions," *Journal of Catalysis*, vol. 325, pp. 145–155, 2015.

[15] Z. Yao, Y. Guo, Y. Yang, H. Huang, and D. Qu, "MnO_x-CeO_x nanoparticles supported on graphene aerogel for selective catalytic reduction of nitric oxides," *Journal of Nanomaterials*, vol. 2019, Article ID 4239764, 9 pages, 2019.

[16] T. Boningari, D. K. Pappas, and P. G. Smirniotis, "Metal oxide-confined interwaeved titania nanotubes M/TNT (M = Mn, Cu, Ce, Fe, V, Cr, and Co) for the selective catalytic reduction of NO_x in the presence of excess oxygen," *Journal of Catalysis*, vol. 365, pp. 320–333, 2018.

[17] J. Lee, O. K. Farha, J. Roberts, K. A. Scheidt, S. T. Nguyen, and J. T. Hupp, "Metal-organic framework materials as catalysts," *Chemical Society Reviews*, vol. 38, no. 5, pp. 1450–1459, 2009.

[18] M. Zhang, J. Guan, B. Zhang, D. Su, C. T. Williams, and C. Liang, "Chemical vapor deposition of $Pd(C_3H_5)(C_5H_5)$ to synthesize Pd@MOF-5 catalysts for suzuki coupling reaction," *Catalysis Letters*, vol. 142, no. 3, pp. 313–318, 2012.

[19] N. Stock and S. Biswas, "Synthesis of metal-organic frameworks (MOFs): routes to various MOF topologies, morphologies, and composites," *Chemical Reviews*, vol. 112, no. 2, pp. 933–969, 2012.

[20] W. Sun, L.-C. Lin, X. Peng, and B. Smit, "Computational screening of porous metal-organic frameworks and zeolites for the removal of SO_2 and NO_x from flue gases," *AIChE Journal*, vol. 60, no. 6, pp. 2314–2323, 2014.

[21] H. Jiang, S. Wang, C. Wang, Y. Chen, and M. Zhang, "Selective catalytic reduction of NO_x with NH_3 on Cu-BTC-derived catalysts: influence of modulation and thermal treatment," *Catalysis Surveys from Asia*, vol. 22, no. 2, pp. 95–104, 2018.

[22] C. Li, Y. Shi, H. Zhang, Q. Zhao, F. Xue, and X. Li, "Cu-BTC metal-organic framework as a novel catalyst for low temperature selective catalytic reduction (SCR) of NO by NH_3: promotional effect of activation temperature," *Integrated Ferroelectrics*, vol. 172, no. 1, pp. 169–179, 2016.

[23] Y.-H. Qin, L. Huang, J.-X. Zheng, and Q. Ren, "Low-temperature selective catalytic reduction of NO with CO over A-Cu-BTC and AO_x/CuO_y/C catalyst," *Inorganic Chemistry Communications*, vol. 72, pp. 78–82, 2016.

[24] M. Kang, E. D. Park, J. M. Kim, and J. E. Yie, "Cu-Mn mixed oxides for low temperature NO reduction with NH_3," *Catalysis Today*, vol. 111, no. 3-4, pp. 236–241, 2006.

[25] B. Thirupathi and P. G. Smirniotis, "Co-doping a metal (Cr, Fe, Co, Ni, Cu, Zn, Ce, and Zr) on Mn/TiO_2 catalyst and its effect on the selective reduction of NO with NH_3 at low-temperatures," *Applied Catalysis B: Environmental*, vol. 110, pp. 195–206, 2011.

[26] D. Fang, J. Xie, D. Mei et al., "Effect of $CuMn_2O_4$ spinel in Cu–Mn oxide catalysts on selective catalytic reduction of NO_x with NH_3 at low temperature," *RSC Advances*, vol. 4, no. 49, pp. 25540–25551, 2014.

[27] W. Wong-Ng, J. A. Kaduk, D. L. Siderius et al., "Reference diffraction patterns, microstructure, and pore-size distribution for the copper (II) benzene-1,3,5-tricarboxylate metal organic framework (Cu-BTC) compounds," *Powder Diffraction*, vol. 30, no. 1, pp. 2–13, 2015.

[28] S. Yong, S. Xiao-Yu, Z. Wang et al., "Synthesis and characterization of Cu^+/MIL-100(Fe) with enhanced catalytic performance for NH_3-SCR," *Ferroelectrics*, vol. 522, no. 1, pp. 20–28, 2018.

[29] F. Kapteijn, A. D. Vanlangeveld, J. A. Moulijn et al., "Alumina-supported manganese oxide catalysts: I. Characterization: effect of precursor and loading," *Journal of Catalysis*, vol. 150, no. 1, pp. 94–104, 1994.

[30] Y. Lu, Y. Lin, T. Xie, S. Shi, H. Fan, and D. Wang, "Enhancement of visible-light-driven photoresponse of Mn/ZnO system: photogenerated charge transfer properties and photocatalytic activity," *Nanoscale*, vol. 4, no. 20, pp. 6393–6400, 2012.

[31] L. W. Yang, X. Wu, G. Huang, T. Qiu, and Y. Yang, "In situ synthesis of Mn-doped ZnO multileg nanostructures and Mn-related Raman vibration," *Journal of Applied Physics*, vol. 97, no. 1, Article ID 014308, 2005.

[32] Y. Xin, H. Li, N. Zhang et al., "Molecular-level insight into selective catalyst reduction of NO_x with NH_3 to N_2 over a highly efficient bi-functional v_a-MnO_x catalyst at low temperature," *ACS Catalysis*, vol. 8, no. 6, pp. 4937–4949, 2018.

[33] K. Schlichte, T. Kratzke, and S. Kaskel, "Improved synthesis, thermal stability and catalytic properties of the metal-organic framework compound $Cu_3(BTC)_2$," *Microporous and Mesoporous Materials*, vol. 73, no. 1-2, pp. 81–88, 2004.

[34] C. Prestipino, L. Regli, J. G. Vitillo et al., "Local structure of framework Cu(II) in HKUST-1 metallorganic framework: spectroscopic characterization upon activation and interaction with adsorbates," *Chemistry of Materials*, vol. 18, no. 5, pp. 1337–1346, 2006.

[35] W. Y. Siew, N. H. H. Abu Bakar, and M. Abu Bakar, "The influence of green synthesis on the formation of various copper benzene-1,3,5-tricarboxylate compounds," *Inorganica Chimica Acta*, vol. 482, pp. 53–61, 2018.

[36] J.-Y. Luo, H. Oh, C. Henry, and W. Epling, "Effect of C_3H_6 on selective catalytic reduction of NO_x by NH_3 over a Cu/zeolite catalyst: a mechanistic study," *Applied Catalysis B: Environmental*, vol. 123-124, pp. 296–305, 2012.

[37] T. Simons, P. Chen, D. Rauch, R. Moos, and U. Simon, "Sensing catalytic conversion: simultanesous DRIFT and impedance spectrscopy for in situ monitoring of NH_3-SCR on zeolites," *Sensors and Actuators B: Chemical*, vol. 224, pp. 492–499, 2016.

[38] G. Gao, J.-W. Shi, Z. Fan, C. Gao, and C. Niu, "MnM_2O_4 microspheres (M = Co, Cu, Ni) for selective catalytic reduction of NO with NH3: comparative study on catalytic activity and reaction mechanism via in-situ diffuse reflectance infrared Fourier transform spectroscopy," *Chemical Engineering Journal*, vol. 325, pp. 91–100, 2017.